Boundary-Layer Meteorol (2010) 134:131–155
DOI 10.1007/s10546-009-9434-y

ARTICLE

Numerical Investigations of Mean Winds Within Canopies of Regularly Arrayed Cubical Buildings Under Neutral Stability Conditions

Takaaki Kono · Tetsuro Tamura · Yasunobu Ashie

Received: 21 July 2008 / Accepted: 22 September 2009 / Published online: 3 November 2009

Abstract Recently, several attempts have been made to model the wind velocity in an urban canopy in order to accurately predict the mixing and transport of momentum, heat, and pollutants within and above the canopy on an urban scale. For this purpose, unverified assumptions made by Macdonald (Boundary-Layer Meteorol 97:25–45, 2000) to develop a model for the profile of the mean wind velocity within an urban canopy have been used. In the present study, in order to provide foundations for improving the urban canopy models, the properties of the spatially-averaged mean quantities used to make these assumptions have been investigated by performing large-eddy simulations (LES) of the airflow around square and staggered arrays of cubical blocks with the following plan area densities: $\lambda_p = 0.05, 0.11, 0.16, 0.20, 0.25$, and 0.33. The LES results confirm that the discrepancy between the spatial average of wind velocity and Macdonald's five-point average of wind velocity can be large in both types of arrays for large λ_p. It is also confirmed that Prandtl's mixing length varies significantly with height within the canopy, contrary to Macdonald's assumption for both types of arrays and for both small and large λ_p. On the other hand, in accordance with Macdonald's assumption, the sectional drag coefficient is found to be almost constant with height except in the case of staggered arrays with high λ_p.

Keywords Large-eddy simulation · Mixing length · Sectional drag coefficient · Spatial average · Urban canopy

T. Kono (✉) · T. Tamura
Department of Environmental Science and Technology, Tokyo Institute of Technology, Nagatsuta 4259, Midori-ku, Yokohama 226-8502, Japan
e-mail: t-kono@kenken.go.jp

T. Kono
Environmental Research Group, Building Research Institute, Tachihara 1, Tsukuba-shi 305-0802, Japan

Y. Ashie
Building Department, National Institute for Land and Infrastructure Management, Tachihara 1, Tsukuba-shi 305-0802, Japan

1 Introduction

When studying the mixing and transport of momentum, heat, and pollutants within and above an urban canopy on an urban scale, it is useful to deal with spatially-averaged physical quantities of a mesh in which buildings are resolved vertically and not horizontally. Recently, Macdonald (2000) modelled the vertical profiles of the spatially-averaged time-mean streamwise wind velocity within homogeneous urban canopies as

$$\langle \overline{u} \rangle (z) = \langle \overline{u} \rangle (h) \exp(a \{z/h - 1\}), \tag{1}$$

where the angle brackets denote a spatially-averaged value, the overbar denotes a time-mean value, z is the coordinate in the vertical direction, h is the canopy height, u is the streamwise wind velocity, and a is called the "attenuation coefficient." In Macdonald's model formulation, buildings were represented as arrays of cubical blocks. Further, the following assumptions were made:

(I) The spatially-averaged wind velocity used for determining the parameter a is approximated by a weighted average of the wind velocities obtained from wind-tunnel measurements at five positions lined up between the centre of the wake and that of the gap (see Fig. 1).
(II) Prandtl's mixing length is constant with height within the urban canopy.
(III) The sectional drag coefficient, i.e., the drag coefficient normalized by the spatially-averaged mean wind velocity at each height, is constant with height within the urban canopy.

From the results obtained by fitting the profiles of the wind velocity calculated by Macdonald's model to those of the five-point average of the measured wind velocity, Macdonald (2000) found that the model worked well for most cases except for arrays with high plan area densities (λ_p) where recirculation vortices behind the rows of cubes produced negative mean velocities at small heights.

Recently, by performing direct numerical simulations (DNS) of the airflow around square and staggered arrays of cubical blocks with $\lambda_p = 0.25$, Coceal et al. (2006) showed that the

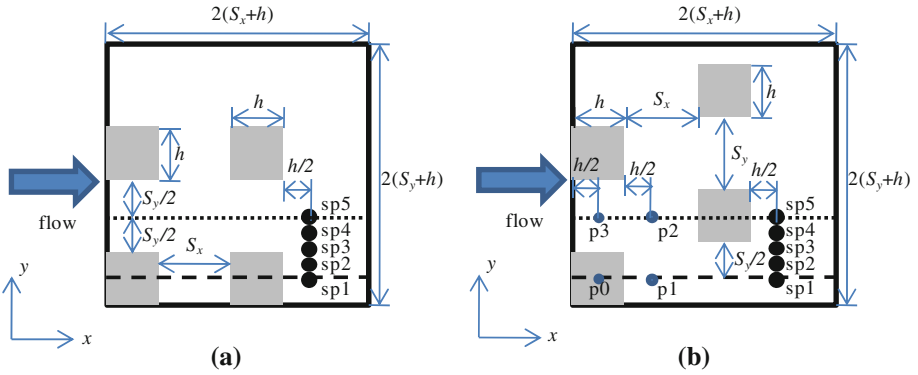

Fig. 1 Schematic plan view of computational domains for **a** a square array and **b** a staggered array of cubical blocks. Here, h is the height of the cubical blocks and the values of $S_x (= S_y)$ are listed in Table 1 with the packing densities of arrays, λ_p. The five-point average of wind velocity (Macdonald 2000) is obtained for points sp1, sp2, sp3, sp4, and sp5 (indicated by *black circles*). Velocity measurements were performed by Cheng and Castro (2002) and Castro et al. (2006) at points p0–p3 (indicated by *blue circles*)

sectional drag coefficient changed drastically at heights below two-fifths of the cube height in the staggered array, and at heights below one-tenth of the cube height in the square array. In addition, they showed that in the former case, Prandtl's mixing length varied significantly inside the canopy as compared to above the canopy; the mixing length increased from the ground to around half the canopy height, and then decreased to the canopy height, having a very small value. Subsequently, it increased with height. Further, by performing DNS for the same arrays, Coceal et al. (2007) showed that the line average of the wind velocity at four positions, which is similar to the five-point average described in assumption I, differed significantly from the spatial average of the wind velocity excluding the space occupied by the blocks (i.e., $\int_{V_f} \overline{u} dV/V_f$, where V_f is the volume of fluid in an averaging cell) in the square array, while the discrepancy was very small at heights above two-fifths of the cube height in the staggered array. From these results, it can be considered that assumptions II and III do not hold well for the staggered array of cubes with $\lambda_p = 0.25$ and that assumption I might not hold well for the square array of cubes with $\lambda_p = 0.25$. However, as mentioned above, it has been confirmed that Macdonald's model does not work well for a large λ_p value of 0.25. Although many numerical investigations of the flow field within arrays of cubical blocks with low λ_p have been conducted, for which Macdonald's model has been considered to work well (e.g., Hanna et al. 2002; Kanda et al. 2004; Hamlyn and Britter 2005; Kanda 2006), the validity of assumptions I, II, and III has not yet been investigated. Nevertheless, these assumptions have been used in some recent attempts to model the wind velocity in urban canopies. For example, Sabatino et al. (2008) used assumptions II and III in their model. In the validation of their model, they noted that a better choice of mixing length might possibly have provided better results. In addition, Coceal and Belcher (2004) used assumption III in their model formulation. Moreover, they used the empirical relation between a, which was obtained based on assumption I, and λ_p of cube arrays in the validation of their model. With regard to the mixing length in urban canopies, they modelled this as a harmonic mean of κz and l_c, considering that, unlike vegetation canopies with a constant mixing length, urban canopies were not "deep" but "shallow," and the mixing length was affected by the ground. Here, κ is the von Karman constant and l_c is a constant mixing length. Further, showing the variation of wind profiles in canopies with λ_p, which were calculated by their model, they concluded that the fact that the mixing lengths were not constant with height in the canopy had the effect that the vertical profiles of wind velocity were not exponential in urban canopies. However, the mixing length calculated by the harmonic mean of κz and l_c increases with height and differs from that obtained by the DNS performed by Coceal et al. (2006) for a staggered array of cubes with $\lambda_p = 0.25$. In addition, as mentioned above, Macdonald's (2000) model has been considered to work well for cube arrays with small λ_p.

On this basis, it can be considered that, over a wide range of λ_p of cube arrays, information on the properties of the spatially-averaged time-mean quantities used to make Macdonald's assumptions I–III will be very useful for the further development of urban canopy models. In this study, we perform large-eddy simulations (LES) of airflow around square and staggered arrays of cubical blocks with $\lambda_p = 0.05, 0.11, 0.16, 0.20, 0.25$, and 0.33, and present a dataset of spatially-averaged time-mean quantities used to make Macdonald's assumptions I–III. In addition, we investigate the extent to which assumptions I–III are accurate, and also discuss explanations for the properties of these spatially-averaged time-mean quantities.

2 Definitions of Spatial Averaging, Mixing Length, and Sectional Drag Coefficient

2.1 Review of Macdonald's (2000) Model

In this study, we use a right-handed rectangular Cartesian coordinate system $x_i(x, y, z)$ with streamwise $x_1(x)$, spanwise $x_2(y)$, and vertical $x_3(z)$ directions. The velocity components are denoted by u_i and they possess streamwise $u_1(u)$, spanwise $u_2(v)$, and vertical $u_3(w)$ components. Vector quantities are indicated by a boldface type, i.e., $(x, y, z) \equiv \boldsymbol{x}$, and spatially-averaged values are denoted by angular brackets.

Macdonald (2000) extended Cionco's (1965) model for mean wind-speed profiles in vegetative canopies to urban canopies. In Macdonald's approach, buildings in urban canopies were treated as two-dimensional cylinders with a sectional drag coefficient $C_D(z)$. Moreover, it was assumed that at each cross-section, there existed a balance between the building's drag force and the local shear stress at each height. The differential drag per unit area is expressed as

$$d\left\langle\overline{\tau}\right\rangle(z) = 0.5\rho C_D(z)\left\langle\overline{u}\right\rangle^2(z) dA_f/A_d, \tag{2}$$

where $d\left\langle\overline{\tau}\right\rangle$ is the change in shear stress, dA_f is the portion of the frontal area of the buildings between levels z and $z+dz$ in an averaging cell, A_d is the plan area of an averaging cell, and ρ is the density of air. Since the cross-section of these buildings is uniform, the following relation holds:

$$dA_f = A_f dz/h, \tag{3}$$

where h is the height of the buildings. Then, Macdonald (2000) approximated the spatially-averaged shear stress by applying Prandtl's mixing-length hypothesis

$$\left\langle\overline{\tau}\right\rangle(z) = \rho\left\{l_m(z) d\left\langle\overline{u}\right\rangle(z)/dz\right\}^2, \tag{4}$$

where l_m is Prandtl's mixing length. Using Eq. 4, Eq. 2 is re-written as

$$\frac{d}{dz}\left\{\left\{l_m(z) d\left\langle\overline{u}\right\rangle(z)/dz\right\}^2\right\} = \sigma_f(z)\left\langle\overline{u}\right\rangle^2(z). \tag{5}$$

Here, σ_f is the friction coefficient defined as

$$\sigma_f(z) = 0.5 C_D(z)\lambda_f/h, \tag{6}$$

where λ_f is the frontal area density defined as

$$\lambda_f = A_f/A_d. \tag{7}$$

Further, Macdonald (2000) assumed that l_m and C_D were constant with height. Under these conditions, a solution that satisfies Eq. 5 is Eq. 1, where

$$a^3 = \frac{h^3\sigma_f}{2l_m^2}. \tag{8}$$

By conducting wind-tunnel measurements of the wind velocity profile at five points in square and staggered arrays of cubical blocks (shown in Fig. 1) with $\lambda_p = 0.05, 0.11, 0.16, 0.20$, and 0.33, Macdonald (2000) calculated the five-point average of the wind velocity at each height using

$$\left\langle u\right\rangle_{5m}(z) = \left\{0.5u_{sp1}(z) + u_{sp2}(z) + u_{sp3}(z) + u_{sp4}(z) + 0.5u_{sp5}(z)\right\}/4, \tag{9}$$

where the subscripted numbers on the right-hand side denote the sampling points indicated in Fig. 1. Then, assuming the five-point average of the wind velocity to be the spatially-averaged wind velocity of a unit area, Macdonald (2000) fitted Eq. 1 to these profiles and found the following empirical relation:

$$a = 9.6\lambda_f. \tag{10}$$

In arrays of cubical blocks, $\lambda_p = \lambda_f$.

2.2 Definition of Spatial Averaging

The mathematical definitions proposed thus far for the spatial average of a flow variable ϕ in canopies or permeable media are divided into two typical types based on the definitions of the domain of integration. The first type excludes the total volume of solids in an averaging cell, V_s, from the domain of integration (hereafter referred to as "solid-exclusive averaging"), and it is expressed as

$$\langle\phi\rangle_{exc1}(\boldsymbol{x}) = \frac{1}{V_f}\int_{V_f}\phi(\boldsymbol{x}+\boldsymbol{x}')d^3\boldsymbol{x}', \tag{11}$$

(e.g., Finnigan 2000) or

$$\langle\phi\rangle_{exc2}(\boldsymbol{x}) = \frac{1}{V_f+V_s}\int_{V_f}\phi(\boldsymbol{x}+\boldsymbol{x}')d^3\boldsymbol{x}', \tag{12}$$

(e.g., Miguel et al. 2001). The second type includes V_s in the domain of integration (hereafter referred to as "solid-inclusive averaging") and is expressed as

$$\langle\phi\rangle_{inc}(\boldsymbol{x}) = \frac{1}{V_f+V_s}\int_{V_f+V_s}\phi(\boldsymbol{x}+\boldsymbol{x}')d^3\boldsymbol{x}', \tag{13}$$

(e.g., Lien et al. 2005). In general, the averaging volume is horizontally extended to a degree sufficient to eliminate variations in canopy structure but made sufficiently thin vertically to preserve the characteristic variation in properties. Above a canopy, there are no differences among $\langle\phi\rangle_{exc1}$, $\langle\phi\rangle_{exc2}$, and $\langle\phi\rangle_{inc}$ because $V_s = 0$. Within a canopy, the following relation holds between $\langle\phi\rangle_{exc1}$ and $\langle\phi\rangle_{exc2}$:

$$\langle\phi\rangle_{exc1} = \frac{V_f+V_s}{V_f}\langle\phi\rangle_{exc2}. \tag{14}$$

If ϕ is assumed to be zero in the space occupied by solid bodies, the values of $\langle\phi\rangle_{inc}$ and $\langle\phi\rangle_{exc2}$ become identical.

As mentioned in the Sect. 1, Coceal et al. (2007) compared a line average of $\overline{u}$ with $\langle\overline{u}\rangle_{exc1}$. However, considering the volume of space that is represented by each point of a line average, it might have been appropriate to compare a line average of $\overline{u}$ with $\langle\overline{u}\rangle_{inc}$. In this study, we mainly use solid-inclusive averaging, except when we focus on the differences among $\langle\overline{u}\rangle_{5m}$, $\langle\overline{u}\rangle_{inc}$, and $\langle\overline{u}\rangle_{exc1}$.

2.3 Definitions of Mixing Length and Sectional Drag Coefficient

Solid-inclusive averaging can be considered as a filtering operation used for LES formulations. Leonard's (1974) spatial filtering of ϕ for a single phase flow in an unbounded domain,

$$\langle\phi\rangle(\boldsymbol{x}) = \int_{-\infty}^{+\infty}\int_{-\infty}^{+\infty}\int_{-\infty}^{+\infty} G(\boldsymbol{x}-\boldsymbol{\xi}, \boldsymbol{\Delta}(\boldsymbol{x}))\phi(\boldsymbol{\xi})d^3\boldsymbol{\xi}, \tag{15}$$

using the top-hat filter with a spatially homogeneous filter width Δ_{x_i},

$$G(\boldsymbol{x}-\boldsymbol{\xi}) = \begin{cases} 1/\Delta_x\Delta_y\Delta_z, & if\ |x_i-\xi_i| < \Delta_{x_i}/2 \\ 0, & \text{otherwise} \end{cases}, \tag{16}$$

is expressed as

$$\langle\phi\rangle(\boldsymbol{x}) = \frac{1}{\Delta_x\Delta_y\Delta_z}\int_{-\Delta_x/2}^{\Delta_x/2}\int_{-\Delta_y/2}^{\Delta_y/2}\int_{-\Delta_z/2}^{\Delta_z/2}\phi(\boldsymbol{x}+\boldsymbol{x}')d^3\boldsymbol{x}'. \tag{17}$$

Equation 17 is mathematically identical to Eq. 13 with an averaging volume $(V_f + V_s)$ of $\Delta_x\Delta_y\Delta_z$. Therefore, from the fundamental properties of a filtering operation with a homogeneous filter width, the following commutation relation holds (e.g., Sagaut 2005):

$$\left\langle\frac{\partial\phi}{\partial x_i}\right\rangle_{inc} - \frac{\partial\langle\phi\rangle_{inc}}{\partial x_i} = 0. \tag{18}$$

By introducing the concept of the immersed boundary method (IBM) (e.g., Fadlun et al. 2000) and applying the solid-inclusive averaging (Eqs. 13 and 18) to the Navier-Stokes equations, we derived the spatially-averaged momentum equations for flow through an urban canopy (Kono et al. 2009a,b). First, we assumed that (i) the entire space, including that occupied by buildings, was filled with a fluid, and (ii) an external body force field existed that always reduced the wind speed to zero at all positions coinciding with the space occupied by the buildings. Under these assumptions, the Navier-Stokes equations are expressed as

$$\frac{\partial u_i}{\partial t} + \frac{\partial u_i u_j}{\partial x_j} = -\frac{1}{\rho}\frac{\partial p}{\partial x_i} + \nu\frac{\partial^2 u_i}{\partial x_j^2} + f_i, \tag{19}$$

and, inside and on the surface of a building,

$$f_i = \frac{1}{\rho}\frac{\partial p}{\partial x_i} - \nu\frac{\partial^2 u_i}{\partial x_j^2} \tag{20a}$$

otherwise,

$$f_i = 0. \tag{20b}$$

Then, by applying solid-inclusive averaging (Eqs. 13 and 18) to Eqs. 19 and 20, the following spatially-averaged equations were derived:

$$\begin{aligned}&\frac{\partial\langle u_i\rangle_{inc}}{\partial t} + \frac{\partial\langle u_i\rangle_{inc}\langle u_j\rangle_{inc}}{\partial x_j} \\ &\quad= -\frac{1}{\rho}\frac{\partial\langle p\rangle_{inc}}{\partial x_i} - \frac{\partial\left\{\langle u_i u_j\rangle_{inc} - \langle u_i\rangle_{inc}\langle u_j\rangle_{inc}\right\}}{\partial x_j} + \nu\frac{\partial^2\langle u_i\rangle_{inc}}{\partial x_j^2} + \langle f_i\rangle_{inc},\end{aligned} \tag{21}$$

$$\langle f_i \rangle_{inc} = \frac{1}{\rho\{V_f + V_s\}} \int_{B_{sb}} p n_i dS - \frac{1}{V_f + V_s} \int_{B_{sb}} \nu \frac{\partial u_i}{\partial n} dS, \tag{22}$$

where B_{sb} is the boundary surface of a building and $\boldsymbol{n}$ is the outward pointing unit normal field of B_{sb} (positive when directed from V_s into V_f). The first and second terms on the right-hand side of Eq. 22 are the form drag and viscous drag, respectively, normalized by the averaging volume.

If we apply solid-inclusive averaging (Eqs. 13 and 18) to the time-averaged Eqs. 19 and 20, the following equations are derived:

$$\frac{\partial \langle \overline{u}_i \rangle_{inc}}{\partial t} + \frac{\partial \langle \overline{u}_i \rangle_{inc} \langle \overline{u}_j \rangle_{inc}}{\partial x_j} = -\frac{1}{\rho} \frac{\partial \langle \overline{p} \rangle_{inc}}{\partial x_i} - \frac{\partial \left\{ \left\langle \overline{u_i' u_j'} \right\rangle_{inc} + \left\langle \overline{u}_i'' \overline{u}_j'' \right\rangle_{inc} \right\}}{\partial x_j} + \nu \frac{\partial^2 \langle \overline{u}_i \rangle_{inc}}{\partial x_j^2} + \langle \overline{f}_i \rangle_{inc}, \tag{23}$$

and

$$\langle \overline{f}_i \rangle_{inc} = \frac{1}{\rho\{V_f + V_s\}} \int_{B_{sb}} \overline{p} n_i dS - \frac{1}{V_f + V_s} \int_{B_{sb}} \nu \frac{\partial \overline{u}_i}{\partial n} dS, \tag{24}$$

where

$$\phi' = \phi - \overline{\phi}, \tag{25}$$

and

$$\phi'' = \phi - \langle \phi \rangle_{inc}. \tag{26}$$

By spatially averaging the results of the large-eddy simulations of the flow around the staggered array of cubes with $\lambda_p = 0.25$, we investigated the budget for the streamwise component of time-averaged Eq. 21 (Kono et al. 2009b) and that of Eq. 23 (Kono et al. 2007). We found that in the budget for the streamwise component of time-averaged Eq. 21, the contributions of $\overline{-\partial \langle uw \rangle_{inc}(z)/\partial z}$ and $\overline{\langle f_1 \rangle_{inc}(z)}$ were dominant within the cube height and balanced against each other, i.e.,

$$\overline{\langle f_1 \rangle_{inc}(z)} \approx \overline{\frac{\partial \langle uw \rangle_{inc}(z)}{\partial z}}. \tag{27}$$

In addition, in the budget for the streamwise component of Eq. 23, the contributions of $-\partial \left\langle \overline{u'w'} \right\rangle_{inc}(z)/\partial z$, $-\partial \left\langle \overline{u}''\overline{w}'' \right\rangle_{inc}(z)/\partial z$, and $\langle \overline{f}_1 \rangle_{inc}(z)$ were dominant within the canopy height and $-\partial \left\{ \left\langle \overline{u'w'} \right\rangle_{inc}(z) + \left\langle \overline{u}''\overline{w}'' \right\rangle_{inc}(z) \right\}/\partial z$ was balanced by $\langle \overline{f}_1 \rangle_{inc}(z)$, i.e.,

$$\langle \overline{f}_1 \rangle_{inc}(z) \approx \frac{\partial \left\{ \left\langle \overline{u'w'} \right\rangle_{inc}(z) + \left\langle \overline{u}''\overline{w}'' \right\rangle_{inc}(z) \right\}}{\partial z}. \tag{28}$$

Therefore, it can be considered that $\langle \overline{\tau} \rangle(z)/\rho$ in Eq. 2 is approximately equal to $-\overline{\langle uw \rangle_{inc}(z)}$ or $-\left\{ \left\langle \overline{u'w'} \right\rangle_{inc}(z) + \left\langle \overline{u}''\overline{w}'' \right\rangle_{inc}(z) \right\}$. In this study, we define $\langle \overline{\tau} \rangle(z)/\rho$ as

$$\frac{\langle \overline{\tau} \rangle(z)}{\rho} = -\overline{\langle uw \rangle_{inc}(z)} \tag{29}$$

for the calculation of $l_m(z)$ in Eq. 4; thus,

$$l_m(z) = \frac{\sqrt{-\overline{\langle uw \rangle_{inc}}(z)}}{d\,\langle \overline{u} \rangle_{inc}\,(z)/dz}. \tag{30}$$

From Eqs. 2, 3, 7, 27, and 29, $C_D(z)$ is expressed as

$$C_D(z) = \frac{-\overline{\langle f_1 \rangle_{inc}\,(z)}h}{0.5\,\langle \overline{u} \rangle_{inc}^2\,(z)\lambda_f}. \tag{31}$$

3 Numerical Approach

3.1 Governing Equations

A filtered continuous equation and the Navier-Stokes equations are used as the governing equations for LES:

$$\frac{\partial u_i^g}{\partial x_i} = 0, \tag{32}$$

$$\frac{\partial u_i^g}{\partial t} + u_j^g \frac{\partial u_i^g}{\partial x_j} = \frac{u_\tau^2}{H}\delta_{i1} - \frac{1}{\rho}\frac{\partial p^g}{\partial x_i} + \nu \frac{\partial u_i^g}{\partial x_j \partial x_j} - \frac{\partial \tau_{ij}^g}{\partial x_j}, \tag{33}$$

where τ_{ij} is the subgrid-scale stress, u_τ is the total wall friction velocity defined as $\{\tau_0/\rho\}^{0.5}$, τ_0 is the wind stress on the ground and the blocks, δ_{ij} is the Kronecker delta, and H is the computational domain height. The superscript g denotes the filtering operation at the grid scale that resolves the cubical blocks. The first term on the right-hand side of Eq. 33 is the driving force of the flow. The subgrid-scale stress τ_{ij} is computed using the dynamic Smagorinsky model of Germano et al. (1991) and Lilly (1992).

3.2 Simulation Set-up

The computational domain, total number of grid points, and u_τ values in Eq. 33 for all run cases are given in Table 1 and Fig. 1. Here, $h = 20\,\mathrm{mm}$ is the height of the cubical block. Cheng and Castro (2002) and Castro et al. (2006) conducted a wind-tunnel experiment for a staggered array of cubes with $\lambda_p = 0.25$ (with a very large number of cubes) and obtained detailed wind data at the four points indicated in Fig. 1b. The height of the computational domain $H(= 7.5h)$ is equivalent to the boundary-layer height of the measurement points. In the wind-tunnel experiment, the free stream velocity U_r was $10\,\mathrm{m\,s^{-1}}$, and the Reynolds number based on U_r, h, and a value of $\nu = 1.54 \times 10^{-5}\,\mathrm{m^2\,s^{-1}}$ (air, 25°C) was approximately 1.3×10^4. The u_τ value was estimated using two different methods by Cheng and Castro (2002); one used a direct drag measurement in which the pressure drag on a cube was measured; the estimated u_τ value was $0.724\,\mathrm{m\,s^{-1}}$. The other used a turbulent shear stress measurement in which the spatially-averaged turbulent shear stress in the inertial and roughness sub-layers was measured; the estimated u_τ value was $0.638\,\mathrm{m\,s^{-1}}$. In the simulation, we use the same value of ν, as described above, in Eq. 33. For a staggered array with $\lambda_p = 0.25$, we use the two different values of u_τ mentioned above in Eq. 33 (these run cases are hereafter referred to as ST25a and ST25b, respectively) to examine the effect of driving forces having different magnitudes. In all run cases, the grid spacing in the x and y directions is $h/32$. The

Table 1 Computational conditions

Array type	Run case	λ_p	$S_x(=S_y)$ in Fig. 1.	Computational domain size	Number of grid points	u_τ[m s^{-1}] in Eq. 33
Square	SQ05	0.05	$3.5h$	$9h \times 9h \times 7.5h$	$288 \times 288 \times 128$	0.7
	SQ11	0.11	$2h$	$6h \times 6h \times 7.5h$	$192 \times 192 \times 128$	0.7
	SQ16	0.16	$1.5h$	$5h \times 5h \times 7.5h$	$160 \times 160 \times 128$	0.7
	SQ20	0.20	$1.25h$	$4.5h \times 4.5h \times 7.5h$	$144 \times 144 \times 128$	0.7
	SQ25	0.25	h	$4h \times 4h \times 7.5h$	$128 \times 128 \times 128$	0.7
	SQ33	0.33	$0.75h$	$3.5h \times 3.5h \times 7.5h$	$112 \times 112 \times 128$	0.57
Staggered	ST05	0.05	$3.5h$	$9h \times 9h \times 7.5h$	$288 \times 288 \times 128$	0.75
	ST11	0.11	$2h$	$6h \times 6h \times 7.5h$	$192 \times 192 \times 128$	0.75
	ST16	0.16	$1.5h$	$5h \times 5h \times 7.5h$	$160 \times 160 \times 128$	0.75
	ST20	0.20	$1.25h$	$4.5h \times 4.5h \times 7.5h$	$144 \times 144 \times 128$	0.73
	ST25a	0.25	h	$4h \times 4h \times 7.5h$	$128 \times 128 \times 128$	0.724
	ST25b	0.25	h	$4h \times 4h \times 7.5h$	$128 \times 128 \times 128$	0.638
	ST33	0.33	$0.75h$	$3.5h \times 3.5h \times 7.5h$	$112 \times 112 \times 128$	0.61

grid spacing in the z direction is $h/32$ from $z = 0$ to $z = 1.5h$, but increases to a maximum of $h/8$ from $z = 1.5h$ to $z = 7.5h$.

A periodic boundary condition is imposed in the x and y directions to simulate an infinite array. At the top of the domain, a free slip condition is imposed for velocity and the Neumann condition is imposed for pressure. At the bottom of the domain and on the surface of the blocks, the conventional no-slip condition and the Neumann condition are imposed for velocity and pressure, respectively.

The governing equations are discretized by the finite difference method on a Cartesian staggered grid system. All spatial derivatives are discretized by the second-order central difference scheme. Time integration is performed using the Adams-Bashforth scheme. The simplified marker and cell (SMAC) method (Amsden and Harlow 1970) is used for velocity–pressure coupling. The Poisson equation for the pressure correction is solved by the biconjugate gradient stabilized (Bi-CGSTAB) method (Van der Vorst 1992).

In all run cases, the initial durations of the runs are approximately $200T$ ($T = h/u_\tau$) and the subsequent durations for measuring statistics are approximately $350T$. These durations are similar to those used in the study of Coceal et al. (2006), in which the validity of these durations was confirmed under a similar simulation setting.

4 Results and Discussion

4.1 Validation of Numerical Approach

In Fig. 2a–f, the vertical profiles of the mean streamwise velocities $\overline{u}$ and the Reynolds shear stresses $-\overline{u'w'}$ of ST25a and ST25b at the four points indicated in Fig. 1b are compared with those of the wind-tunnel measurements of Castro et al. (2006). Further, in Fig. 2g, the vertical profiles of the laterally integrated pressure difference between the front and back faces of the cubical block calculated by ST25a and ST25b are compared with that obtained

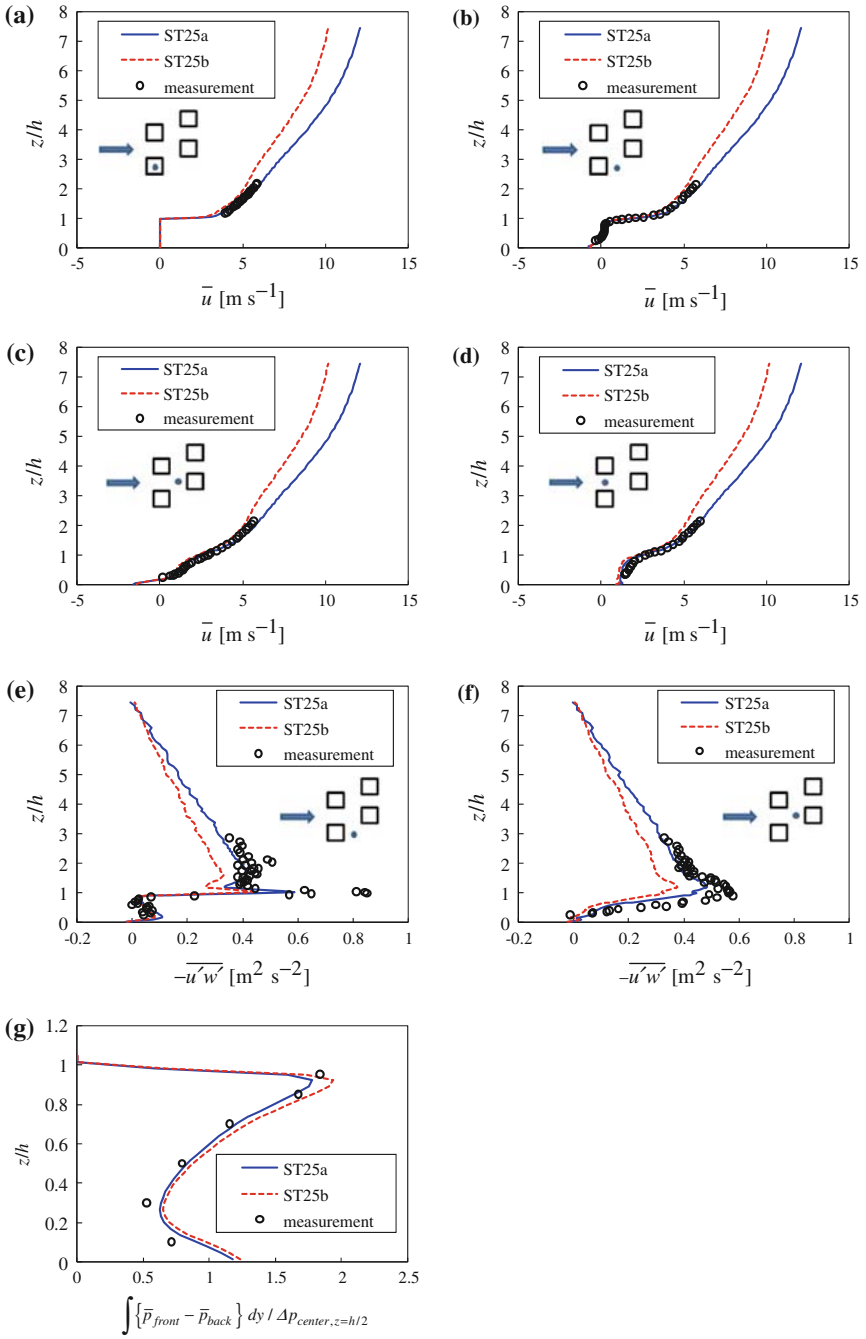

Fig. 2 Comparison of the LES results with the measurements obtained in the wind-tunnel experiment of Cheng and Castro (2002) and Castro et al. (2006) for the staggered array of cubes with $\lambda_p = 0.25$: **a** $\overline{u}$ at p0 in Fig. 1b, **b** $\overline{u}$ at p1 in Fig. 1b, **c** $\overline{u}$ at p2 in Fig. 1b, **d** $\overline{u}$ at p3 in Fig. 1b, **e** $-\overline{u'w'}$ at p1 in Fig. 1b, **f** $-\overline{u'w'}$ at p2 in Fig. 1b, and **g** laterally integrated time-mean pressure difference between the front and back faces of the cube. Here, $\Delta p_{center,z=h/2}$ denotes the time-mean pressure difference between the centres of the front and back faces of the cube

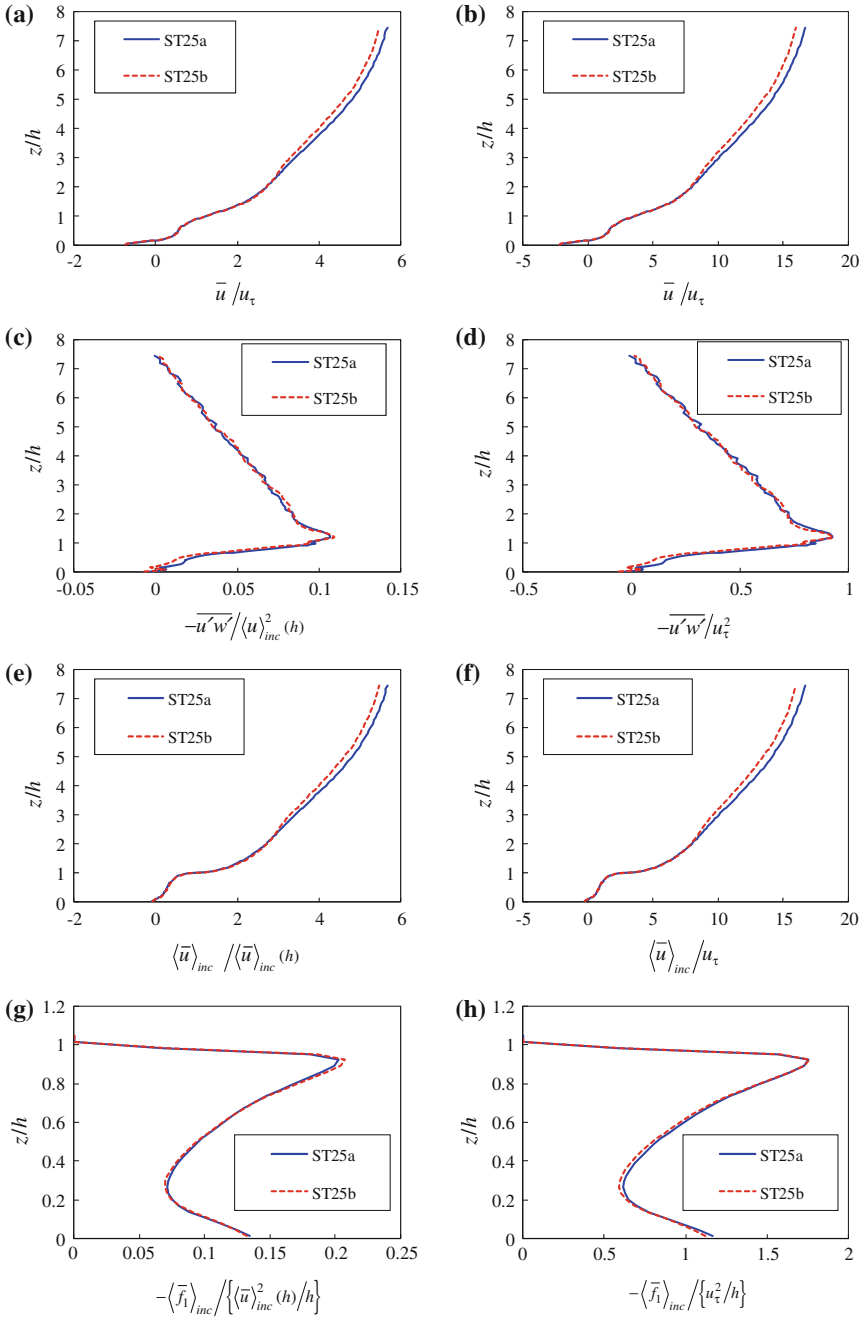

Fig. 3 Vertical profiles of flow quantities normalized by $\langle\overline{u}\rangle_{inc}(h)$ and u_τ for the staggered array of cubes with $\lambda_p = 0.25$: **a** $\overline{u}/\langle\overline{u}\rangle_{inc}(h)$ at p2 in Fig. 1b, **b** $\overline{u}/u_\tau$ at p2 in Fig. 1b, **c** $-\overline{u'w'}/\langle\overline{u}\rangle^2_{inc}(h)$ at p2 in Fig. 1b, **d** $-\overline{u'w'}/u_\tau^2$ at p2 in Fig. 1b, **e** $\langle\overline{u}\rangle_{inc}/\langle\overline{u}\rangle_{inc}(h)$, **f** $\langle\overline{u}\rangle_{inc}/u_\tau$, **g** $-\langle\overline{f}_1\rangle_{inc}/\left\{\langle\overline{u}\rangle^2_{inc}(h)/h\right\}$, and **h** $-\langle\overline{f}_1\rangle_{inc}/\left\{u_\tau^2/h\right\}$

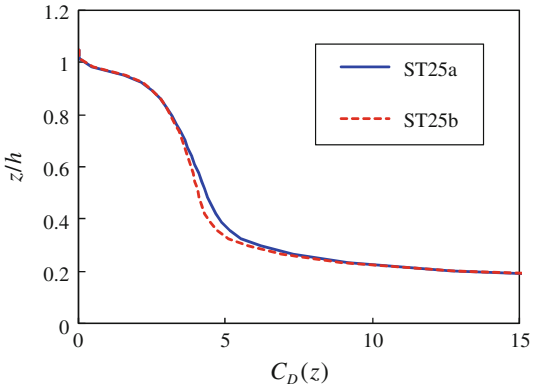

Fig. 4 Vertical profiles of $C_D(z)$ for the staggered array with $\lambda_p = 0.25$

in the wind-tunnel measurements of Cheng and Castro (2002). Here, the measurement data shown are those of Cheng and Castro (2002) taken from Coceal et al. (2006). From Fig. 2, it can be confirmed that all the profiles of ST25a are in good agreement with the wind-tunnel measurements, while the discrepancies between the values calculated by ST25b and ST25a are not always negligible, particularly in the profiles of $-\overline{u'w'}$. Therefore, in order to simulate the flows within and immediately above the arrays of blocks by this approach that uses a driving force, as in Eq. 33, it is considered more appropriate to use the value of u_τ obtained using the direct drag measurement rather than that obtained using the turbulent shear stress measurement. However, if $\overline{u}$, $-\overline{u'w'}$, and $-\overline{\langle f_1 \rangle_{inc}}$ calculated by ST25a and ST25b are normalized by the spatially-averaged wind velocity at the height of the blocks $\langle \overline{u} \rangle_{inc}(h)$, or by u_τ, the profiles become almost identical to each other, especially within and immediately above the block height, as shown in Fig. 3. In addition, as shown in Fig. 4, the vertical profiles of $C_D(z)$ of ST25a and ST25b are almost identical to each other.

From these results, we can understand that different values of the driving force in Eq. 33, within the range of ST25a and ST25b, have a negligible effect on the profiles of $C_D(z)$ and normalized $\langle \overline{u} \rangle_{inc}$ and $\left\langle -\overline{u'w'} \right\rangle_{inc}$ by $\langle \overline{u} \rangle_{inc}(h)$ or u_τ, all of which appear in the derivation of Macdonald's model. Since there exist discrepancies between the actual conditions of the wind-tunnel experiment and the simulation settings such as the upper boundary conditions, $\overline{u}$ of ST25a and ST25b at the top of the computational domain ($z/h = 7.5$) have values of 12.1 and 10.2 m s^{-1}, respectively, and these are different from $U_r (= 10\,\mathrm{m\,s^{-1}})$. The Reynolds numbers of ST25a and ST25b based on these velocities and h are approximately 1.57×10^4 and 1.32×10^4, respectively. In addition, the Reynolds number of Macdonald's (2000) wind-tunnel measurements, approximately 1.46×10^4 based on an upper free stream velocity of 2.25 m s^{-1} and a cube height of 0.1 m, falls in the range of ST25a to ST25b. The u_τ values shown in Table 1 were decided such that $\overline{u}$ at the top of the computational domain was in the range of 10–12 m s^{-1}. Therefore, it is possible to investigate the properties of the spatially-averaged mean quantities used to make assumptions I–III by dealing with the abovementioned normalized quantities with sufficient grid resolution, without considering the effect of different Reynolds numbers. In addition, it is possible to compare the profiles of $\langle \overline{u} \rangle_{5m}$ obtained by LES and Macdonald's (2000) wind-tunnel measurement for Reynolds numbers of the same order.

Figure 5 shows comparisons of the LES results and Macdonald's (2000) wind-tunnel experimental results for $\langle \overline{u} \rangle_{5m}$ (the five points that are indicated in Fig. 1) normalized by $\langle \overline{u} \rangle_{5m}$ of the cube height for square and staggered arrays with $\lambda_p = 0.05, 0.11, 0.16, 0.20,$

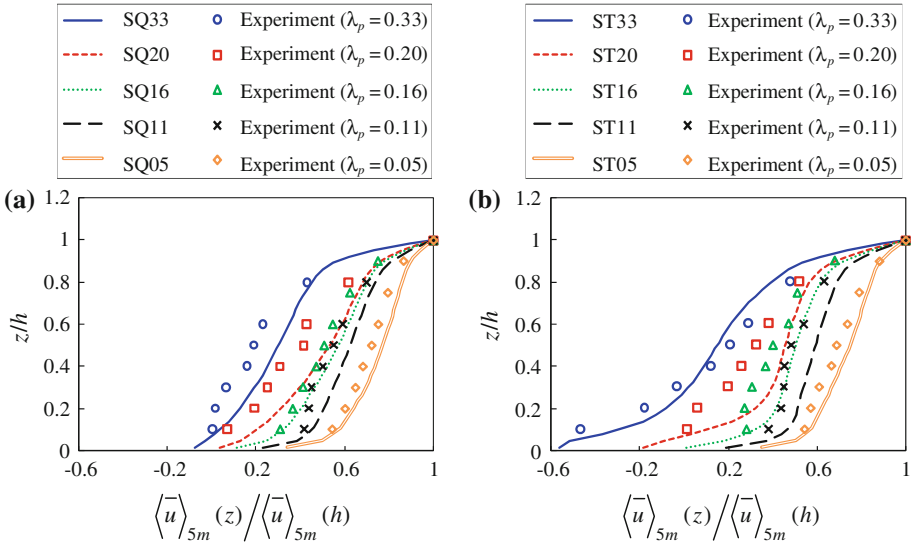

Fig. 5 Vertical profiles of simulated and observed (Macdonald's (2000) wind-tunnel experiment) $\langle\overline{u}\rangle_{5m}(z)/\langle\overline{u}\rangle_{5m}(h)$: **a** square arrays and **b** staggered arrays

and 0.33. Although there exist several large discrepancies between the LES results and the wind-tunnel results, both results exhibit qualitatively similar features, namely, the value of $\langle\overline{u}\rangle_{5m}/\langle\overline{u}\rangle_{5m}(h)$ reduces with an increase in λ_p and a decrease in the distance between z and the ground. The discrepancies may be attributable to the use of $\langle\overline{u}\rangle_{5m}(h)$ for normalizing $\langle\overline{u}\rangle_{5m}$. Since any grid point for u does not coincide with $z = h$ in this simulation setting, we calculated $\langle\overline{u}\rangle_{5m}(h)$ by interpolating $\langle\overline{u}\rangle_{5m}(63h/64)$ and $\langle\overline{u}\rangle_{5m}(65h/64)$. Considering the fact that $\overline{u}$ changes drastically and measurements become difficult in the vicinity of $z = h$, it can be considered that the use of the spatially-averaged $\overline{u}$ at $z = h$ for normalization is not appropriate. Therefore, in the following discussion, we use u_τ for the normalization of the spatially-averaged quantities.

4.2 Investigation of Spatially-Averaged Quantities used in Macdonald's Assumptions

4.2.1 Five-Point Average and Spatial Average

Figure 6 shows comparisons among LES results for $\langle\overline{u}\rangle_{5m}/u_\tau$, $\langle\overline{u}\rangle_{inc}/u_\tau$, and $\langle\overline{u}\rangle_{exc}/u_\tau$ for square and staggered arrays with $\lambda_p = 0.05, 0.11, 0.16, 0.20, 0.25$, and 0.33. In arrays with $\lambda_p = 0.25$, at heights above $z/h = 0.3$, the discrepancies between $\langle\overline{u}\rangle_{5m}/u_\tau$ and $\langle\overline{u}\rangle_{exc}/u_\tau$ (hereafter referred to as "DIS_5m_exc") are significantly large for the square array (SQ25) and very small for the staggered array (ST25a); at heights below $z/h = 0.3$, DIS_5m_exc values are significantly large in both arrays. As mentioned in Sect. 1, Coceal et al. (2007) showed similar tendencies for their DNS results of a line average of $\overline{u}$ at four positions. On the other hand, at heights above $z/h = 0.3$, the discrepancies between $\langle\overline{u}\rangle_{5m}/u_\tau$ and $\langle\overline{u}\rangle_{inc}/u_\tau$ (hereafter referred to as "DIS_5m_inc") are not significantly large for SQ25 (as compared to DIS_5m_exc values) and are relatively large for ST25a (as compared to DIS_5m_exc values); at heights below $z/h = 0.3$, DIS_5m_inc values are significantly large in both arrays as in the case of DIS_5m_exc values.

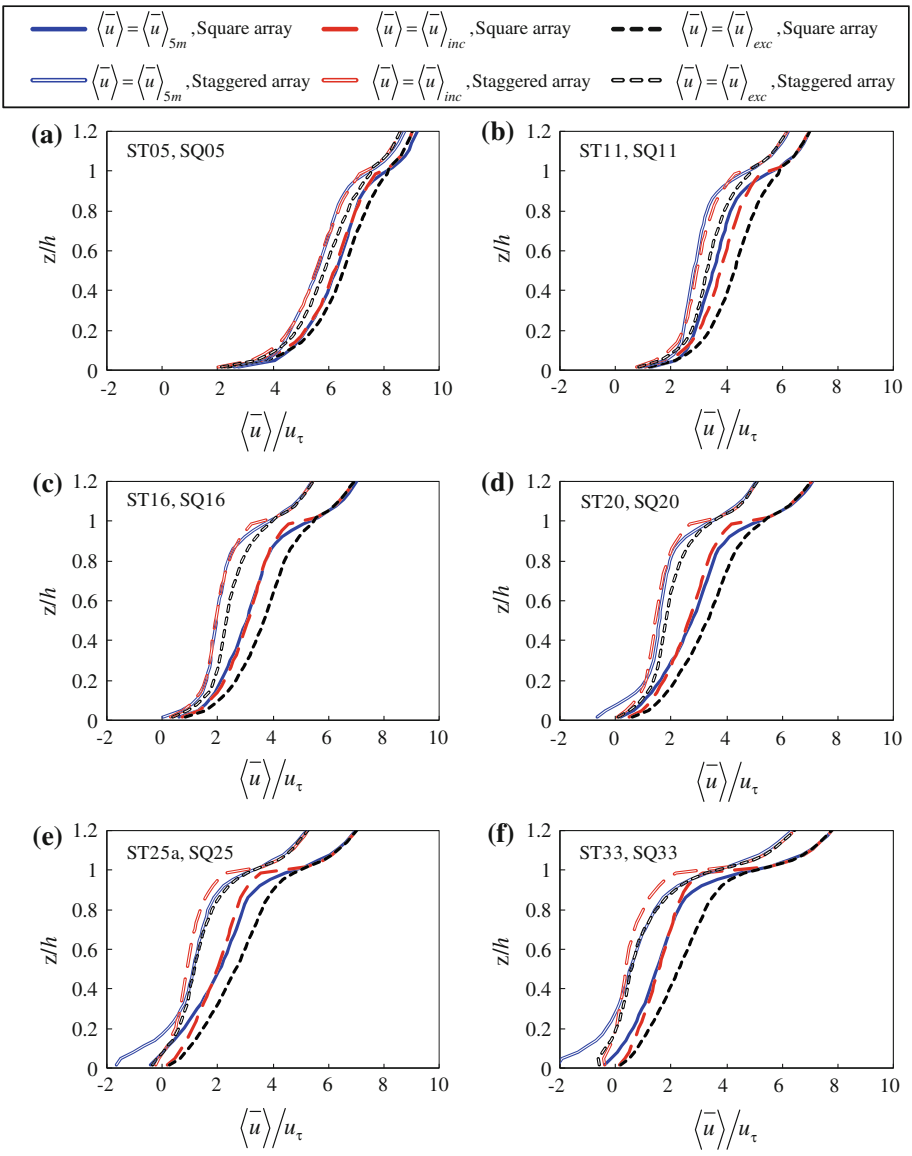

Fig. 6 Vertical profiles of $\langle\overline{u}\rangle_{5m}/u_\tau$, $\langle\overline{u}\rangle_{inc}/u_\tau$, and $\langle\overline{u}\rangle_{exc}/u_\tau$: **a** ST05 and SQ05, **b** ST11 and SQ11, **c** ST16 and SQ16, **d** ST20 and SQ20, **e** ST25a and SQ25, and **f** ST33 and SQ33

In staggered arrays with $\lambda_p \leq 0.20$ and in all square arrays, DIS_5m_exc values are significantly large and greater than DIS_5m_inc values. From these results, together with the volume of the space represented by each point of the five-point average, it is reasonable to consider that $\langle\overline{u}\rangle_{5m}$ is an approximation of $\langle\overline{u}\rangle_{inc}$ rather than $\langle\overline{u}\rangle_{exc}$, and the larger values of DIS_5m_inc values as compared to DIS_5m_exc values in ST25a and ST33 are due to other factors.

The reason why $\langle\overline{u}\rangle_{5m}/u_\tau$ is larger than $\langle\overline{u}\rangle_{inc}/u_\tau$ in staggered arrays with high λ_p (e.g., ST25a) above $z/h = 0.3$ can be understood from Fig. 7a. Points sp1, sp2, and sp3 of the five-point average can be considered to represent area 1 ($0 \leq x/h \leq 2, 0.475 \leq y/h \leq 0.625$),

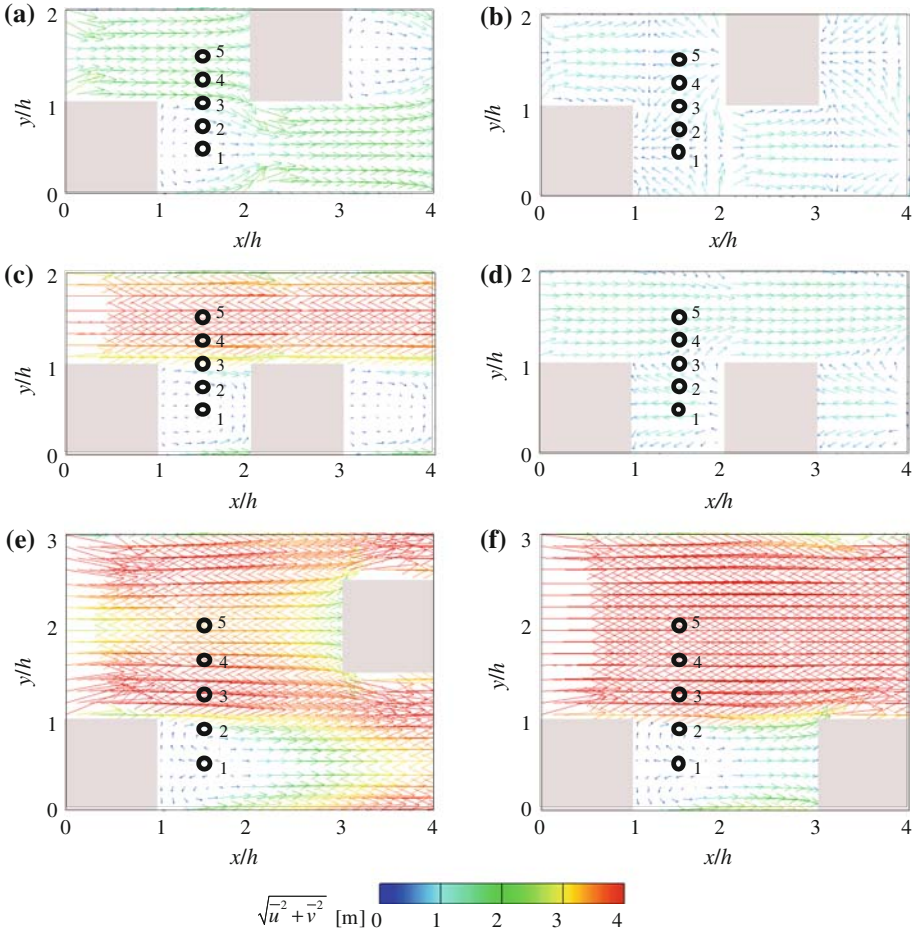

Fig. 7 Horizontal distributions of time-mean two-dimensional wind vectors $(\overline{u}, \overline{v})$: **a** ST25 at $z/h = 0.8$, **b** ST25 at $z/h = 0.06$, **c** SQ25 at $z/h = 0.8$, **d** SQ25 at $z/h = 0.06$, **e** ST11 at $z/h = 0.8$, and **f** SQ11 at $z/h = 0.8$. The prevailing flow is to the right. The wind vectors are plotted at quarter resolution for greater clarity

area 2 ($0 \leq x/h \leq 2, 0.625 \leq y/h \leq 0.875$) and area 3 ($0 \leq x/h \leq 2, 0.875 \leq y/h \leq 1.125$), respectively. Since points sp1–3 are in the area of forward flow, the three-point average of $\overline{u}$ is larger than its solid-inclusive average in the combined area of areas 1–3 due to zero speed in the space occupied by the block. This is the main reason why $\langle\overline{u}\rangle_{5m}/u_\tau$ is larger than $\langle\overline{u}\rangle_{inc}/u_\tau$ in staggered arrays with high λ_p above $z/h = 0.3$. On the other hand, below $z/h = 0.3$, all points of the five-point average are in the area of reverse flow due to the vortices in the wake of the block and in front of the block, as shown in Fig. 7b. This results in $\langle\overline{u}\rangle_{5m}/u_\tau$ having a strong negative value, while $\langle\overline{u}\rangle_{inc}/u_\tau$ has a moderate negative value due to $\overline{u}$ with positive values in the gap area ($0 \leq x/h \leq 1, 1 \leq y/h \leq 2$) and zero speed in the space occupied by the block. For the square arrays with high λ_p, the reason why $\langle\overline{u}\rangle_{5m}/u_\tau$ is larger than $\langle\overline{u}\rangle_{inc}/u_\tau$ around $z/h = 0.8$ and smaller than $\langle\overline{u}\rangle_{inc}/u_\tau$ near the ground can be explained in the same manner using points sp1–3 in Fig. 7c, d.

With a decrease in λ_p for both the staggered and square arrays, DIS_5m_inc values become negligibly small, as shown in Fig. 6c; then $\langle\overline{u}\rangle_{5m}/u_\tau$ becomes smaller than $\langle\overline{u}\rangle_{inc}/u_\tau$, as

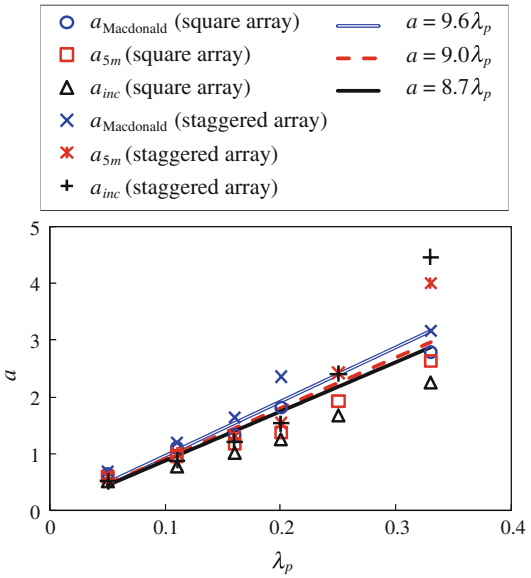

Fig. 8 Variation of attenuation coefficient with λ_p of the cube arrays. Here, $a = 9.6\lambda_p$ is Eq. 10, and $a = 9.0\lambda_p$ and $a = 8.7\lambda_p$ are the least-squares lines for a_{5m} and a_{inc}, respectively

shown in Fig. 6b. This is caused by the development of a reverse flow region in the wake of the block; as shown in Fig. 7e, f, point sp1 lies in the reverse flow region. On the other hand, since the number of points of the five-point average in the wake of the block decreases with a decrease in λ_p, the contribution of the points in the wake of the block becomes less significant. As a result, DIS_5m_inc values become negligibly small again as shown in Fig. 6a.

From the discussions above, it can be understood that the five-point average is significantly affected by the formation of the reverse flow region around the block, especially, in cube arrays with high λ_p.

Figure 8 shows the variation of $a_{\mathrm{Macdonald}}$, a_{5m}, and a_{inc}, which are the attenuation coefficients in Table 1 of Macdonald (2000) and those obtained by the least-squares fit of Eq. 1 to the profiles of $\langle\overline{u}\rangle_{5m}$ and $\langle\overline{u}\rangle_{inc}$, respectively, with λ_p of arrays of cubical blocks. As mentioned earlier, the use of the spatially-averaged $\overline{u}$ at $z = h$ for normalization might not be appropriate; however, at least the following tendencies have been confirmed. Overall, the values of a_{5m} are smaller than those of $a_{\mathrm{Macdonald}}$ because the LES results for $\langle\overline{u}\rangle_{5m}(z)/\langle\overline{u}\rangle_{5m}(h)$ are generally greater than the wind-tunnel experimental results for $\langle\overline{u}\rangle_{5m}(z)/\langle\overline{u}\rangle_{5m}(h)$, as shown in Fig. 5. In addition, the values of a_{inc} are generally smaller than those of a_{5m}. However, the discrepancies among $a_{\mathrm{Macdonald}}$, a_{5m}, and a_{inc} are not significant, especially for arrays with low λ_p, and a_{5m} and a_{inc} can be approximated by straight lines with slopes similar to that of $a_{\mathrm{Macdonald}}$. Therefore, it can be considered that the linear relationships between the attenuation coefficients and λ_p of arrays of cubical blocks are not significantly affected by the discrepancies between $\langle\overline{u}\rangle_{5m}$ and $\langle\overline{u}\rangle_{inc}$.

Table 2 shows $\Delta_{\mathrm{Macdonald}}$, Δ_{5m}, and Δ_{inc}, which are the maximum absolute residuals between $\exp(a_{\mathrm{Macdonald}}\{z/h-1\})$ and the wind-tunnel experimental results of $\langle\overline{u}\rangle_{5m}(z)/\langle\overline{u}\rangle_{5m}(h)$, between $\exp(a_{5m}\{z/h-1\})$ and the LES results of $\langle\overline{u}\rangle_{5m}(z)/\langle\overline{u}\rangle_{5m}(h)$, and between $\exp(a_{inc}\{z/h-1\})$ and $\langle\overline{u}\rangle_{inc}(z)/\langle\overline{u}\rangle_{inc}(h)$, respectively for $z/h > 0.3$; Δ_{5m} tends to be larger than Δ_{inc} in cube arrays with low λ_p, and smaller than Δ_{inc} in cube arrays with high λ_p.

Table 2 Values of the maximum absolute residuals for $\exp(a_{\mathrm{Macdonald}}\{z/h-1\})$, $\exp(a_{5m}\{z/h-1\})$, and $\exp(a_{inc}\{z/h-1\})$ for $z/h > 0.3$

Array type	λ_p	$\Delta_{\mathrm{Macdonald}}$	Δ_{5m}	Δ_{inc}
Square	0.05	0.08	0.06	0.03
	0.11	0.11	0.10	0.07
	0.16	0.13	0.11	0.10
	0.20	0.08	0.11	0.12
	0.25	–	0.13	0.18
	0.33	0.15	0.20	0.25
Staggered	0.05	0.05	0.06	0.03
	0.11	0.16	0.14	0.09
	0.16	0.18	0.17	0.13
	0.20	0.11	0.19	0.17
	0.25	–	0.16	0.21
	0.33	0.06	0.11	0.24

4.2.2 Mixing Length

Figure 9a, b show the vertical profiles of l_m/h, which is calculated from Eq. 30, for square and staggered arrays, respectively, for $\lambda_p = 0.05, 0.11, 0.16, 0.20, 0.25$, and 0.33. As seen in the figures, the values of l_m/h change significantly in the canopy even for arrays with low λ_p. As compared to the magnitudes of l_m/h at $z/h = 2.0$, it is difficult to consider the degrees of these changes in the canopies to be constant with height.

Table 3 shows the maximum and height-averaged values of l_m/h in the canopies, together with the values of l_m/h estimated by Macdonald (2000) using the following two different relations derived based on several assumptions:

$$l_m/h = \sqrt{\overline{C_{DH}}\lambda_f\left\{1-e^{-2a}\right\}/\left\{4a^3\right\}}, \tag{34}$$

and

$$l_m/h = a^{-1}u_\tau/u_h, \tag{35}$$

where $\overline{C_{DH}}$ is the height-mean drag coefficient and a value of 1.2 was used based on the typical value for the height-mean drag coefficient of surface-mounted cubes in a shear flow (ESDU 1986). It should be noted that, while the values of l_m/h, which are estimated from Eqs. 34 and 35, respectively, increase monotonically as λ_p decreases, the maximum and height-averaged values of l_m/h in the canopies obtained by the LES have a peak at $\lambda_p = 0.11$ for square arrays and at $\lambda_p = 0.20$ for staggered arrays. Between this and a lower value of λ_p, the maximum and height-averaged values of l_m/h decrease monotonically in both square and staggered arrays. Since the discrepancies between the maximum value of l_m/h and the height-averaged value of l_m/h also decrease monotonically as λ_p decreases from $\lambda_p = 0.16$ in square arrays and $\lambda_p = 0.20$ in staggered arrays, it can be considered that l_m/h tends to be less variable with height as λ_p decreases in cube arrays with low λ_p.

The values of l_m/h become very small at the height of the canopy ($z/h = 1.0$) because the values of $\left\{d\overline{\langle u\rangle}_{inc}/dz\right\}h/u_\tau$ are significantly large at this height, as shown in Fig. 9c, d, although the values of $\sqrt{-\overline{\langle uw\rangle}_{inc}}/u_\tau$ are maximum around this height, as shown in Fig. 9e, f, and turbulent mixing is significantly active. These significantly large values of

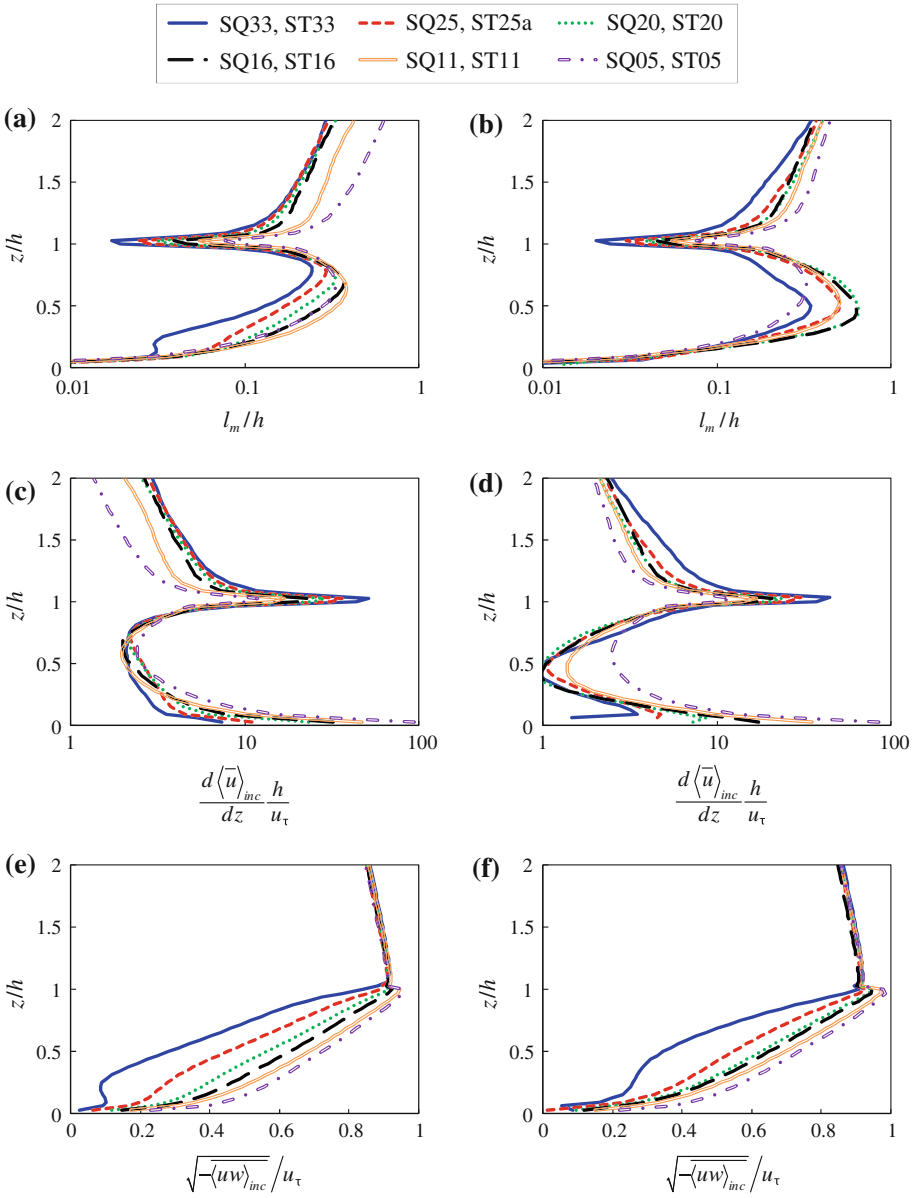

Fig. 9 Vertical profiles of l_m/h, $d\langle\overline{u}\rangle_{inc}/dz \cdot h/u_\tau$, and $\sqrt{-\overline{\langle uw\rangle_{inc}}}/u_\tau$: **a** l_m/h in square arrays, **b** l_m/h in staggered arrays, **c** $d\langle\overline{u}\rangle_{inc}/dz \cdot h/u_\tau$ in square arrays, **d** $d\langle\overline{u}\rangle_{inc}/dz \cdot h/u_\tau$ in staggered arrays, **e** $\sqrt{-\overline{\langle uw\rangle_{inc}}}/u_\tau$ in square arrays, and **f** $\sqrt{-\overline{\langle uw\rangle_{inc}}}/u_\tau$ in staggered arrays

$\left\{d\overline{\langle u\rangle_{inc}}/dz\right\} h/u_\tau$ occur due to the sharp decline in the wind speed above the cubical blocks towards the blocks' top surfaces. In Fig. 10, which shows the time-mean spanwise vorticity contours in the vertical x–z planes for ST25a, SQ25, ST11, and SQ11, it is confirmed that strong shear layers at around $z/h = 1$ exist only in the x–z planes that intersect the cubical

Table 3 Values of the maximum and height-averaged mixing lengths in the canopies obtained by large-eddy simulation and values of mixing-lengths estimated by Macdonald's (2000) equations (Eqs. 34 and 35)

Array type	λ_p	l_m/h (maximum)	l_m/h (height-average)	l_m/h (Eq. 34)	l_m/h (Eq. 35)
Square	0.05	0.33	0.20	0.21	0.23
	0.11	0.38	0.23	0.15	0.18
	0.16	0.37	0.21	0.14	0.17
	0.20	0.33	0.18	0.10	0.13
	0.25	0.29	0.15	–	–
	0.33	0.24	0.12	0.07	0.09
Staggered	0.05	0.33	0.21	0.18	0.26
	0.11	0.51	0.30	0.13	0.24
	0.16	0.63	0.35	0.10	0.19
	0.20	0.65	0.36	0.07	0.15
	0.25	0.50	0.28	–	–
	0.33	0.34	0.19	0.06	0.11

blocks, regardless of the array type or λ_p. Since momentum is transported into the canopy space excluding the space occupied by the cubical blocks, the wind speed immediately above the blocks' top surfaces is much higher than that immediately above a flat surface, leading to the formation of the strong shear layers above the blocks. The contribution of these shear layers to $\left\{d\overline{\langle u\rangle}_{inc}/dz\right\}h/u_\tau$ decreases with a decrease in λ_p, i.e., a decrease in the ratio of the blocks' top surfaces in an averaging volume; as shown in Fig. 9c, d, the peak value of $\left\{d\overline{\langle u\rangle}_{inc}/dz\right\}h/u_\tau$ at around $z/h = 1$ decreases monotonically with a decrease in λ_p. On the other hand, as shown in Fig. 9e, f, the values of $\sqrt{-\overline{\langle uw\rangle}_{inc}}/u_\tau$ are almost independent of λ_p above the canopy, and they increase monotonically within the canopy with a decrease in λ_p. Here, it is important to note that the blocks' top surfaces suppress the turbulent mixing, and the strong shear layers above the blocks' top surfaces do not contribute to the increase in $\sqrt{-\overline{\langle uw\rangle}_{inc}}/u_\tau$. Therefore, the value of l_m/h at around $z/h = 1$ becomes very small and increases monotonically with a decrease in λ_p.

For a staggered array with $\lambda_p = 0.25$, Coceal et al. (2006) computed the mixing length, which was defined as

$$l_{m\_coceal}(z) = \frac{\sqrt{-\left\langle\overline{u'w'}\right\rangle_{exc}(z)}}{d\left\langle\overline{u}\right\rangle_{exc}(z)/dz}, \tag{36}$$

from their DNS data, and obtained a profile similar to l_m in Fig. 9b. They considered that the small value of l_{m_coceal} at the canopy height indicated that, in an average sense, energetic large eddies were blocked from penetrating the canopy by the strong shear layer over the top of the blocks. This speculation is considered to be reasonable, since the shear layers over the top of the blocks are formed as a result of the no-slip condition over the blocks' surface. In addition, the shear layers separate from the blocks' top surfaces and suppress the momentum transport into the canopy; for instance, at $x/h = 1.5$ in Fig. 10a, $\overline{u}$ and $-\overline{u'w'}$ decrease sharply in the $-z$ direction immediately below the shear layer as shown in Fig. 2b, e, respectively. On the other hand, at $x/h = 3.5$ in Fig. 10a where the separated shear layer does not reach, $\overline{u}$ and $-\overline{u'w'}$ decrease moderately along the $-z$ direction as shown in Fig. 2c,

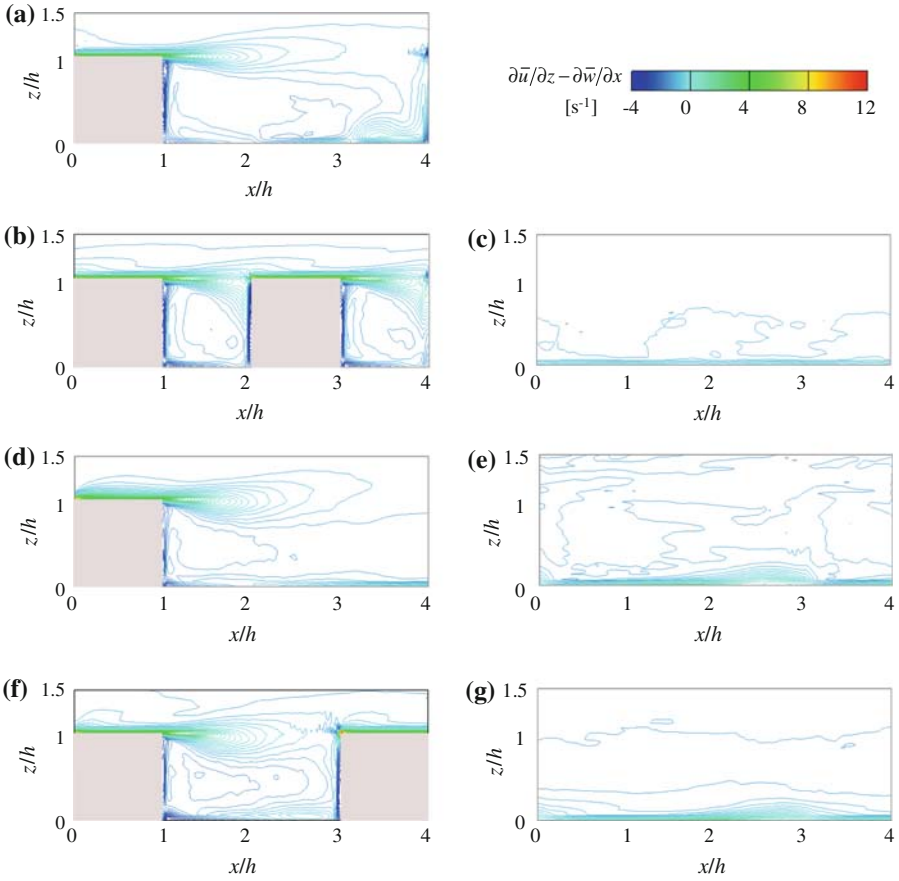

Fig. 10 Spanwise vorticity contours in vertical x–z planes: **a** ST25a at $y/h = 0.5$ in Fig. 7a, **b** SQ25 at $y/h = 0.5$ in Fig. 7c, **c** SQ25 at $y/h = 1.5$ in Fig. 7c, **d** ST11 at $y/h = 0.5$ in Fig. 7e, **e** ST11 at $y/h = 1.25$ in Fig. 7e, **f** SQ11 at $y/h = 0.5$ in Fig. 7f, and **g** SQ11 at $y/h = 1.25$ in Fig. 7f

f, respectively. Therefore, with a decrease in λ_p, the ratio of the space in which strong shear layers exist to an averaging volume decreases, and $\sqrt{-\overline{\langle uw\rangle_{inc}}}/u_\tau$ increases monotonically within the canopy.

Since $\sqrt{-\overline{\langle uw\rangle_{inc}}}/u_\tau$ increases monotonically with a decrease in λ_p, it is understood (from Fig. 9) that the maximum and height-averaged values of l_m/h in the canopies have a peak at $\lambda_p = 0.11$ for square arrays and at $\lambda_p = 0.20$ for staggered arrays, because $\left\{d\overline{\langle u\rangle}_{inc}/dz\right\} h/u_\tau$ increases monotonically with a decrease in λ_p from SQ11 and ST20.

4.2.3 Sectional Drag Coefficient

Figure 11a, b shows $C_D(z)$ for square and staggered arrays, respectively, with $\lambda_p = 0.05, 0.11, 0.16, 0.20, 0.25$, and 0.33. In square arrays with $\lambda_p \leq 0.25$, the values of $C_D(z)$ are almost constant with height above $z/h \approx 0.1$. In staggered arrays, the degrees of change in the values of $C_D(z)$ decrease as λ_p becomes lower and the values of $C_D(z)$ can

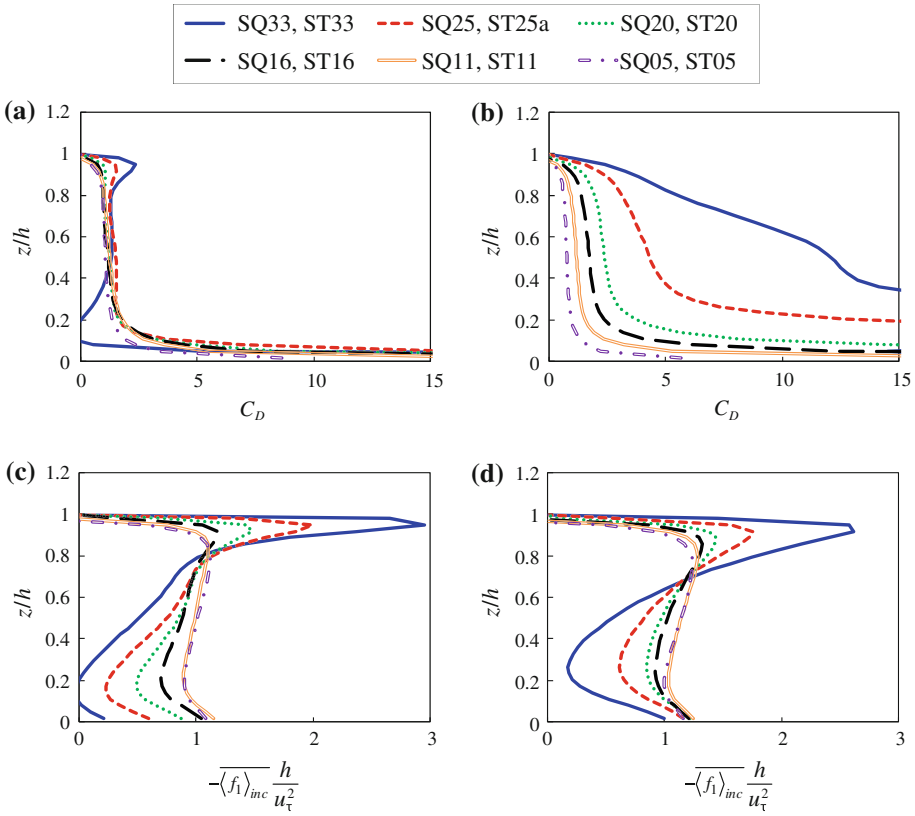

Fig. 11 Vertical profiles of C_D and $-\overline{\langle f_1 \rangle_{inc}}/\left\{u_\tau^2/h\right\}$: **a** C_D in square arrays, **b** C_D in staggered arrays, **c** $-\overline{\langle f_1 \rangle_{inc}}/\left\{u_\tau^2/h\right\}$ in square arrays, and **d** $-\overline{\langle f_1 \rangle_{inc}}/\left\{u_\tau^2/h\right\}$ in staggered arrays

be considered to be almost constant with height above $z/h \approx 0.2$ for $\lambda_p \leq 0.20$. It can be confirmed that the values of $C_D(z)$ in the square arrays are insensitive to λ_p, while those in the staggered arrays are sensitive to λ_p.

The reason why the values of $C_D(z)$ in the staggered arrays are more sensitive to λ_p than those in the square arrays is explained from the balance between the numerator and denominator of the right-hand side of Eq. 31. In Fig. 11c, d, which shows $-\overline{\langle f_1 \rangle_{inc}}/\left\{u_\tau^2/h\right\}$ for square and staggered arrays, respectively, with $\lambda_p = 0.05, 0.11, 0.16, 0.20, 0.25$, and 0.33, it is confirmed that, except for those values at around $z/h \approx 0.95$ in arrays with $\lambda_p \geq 0.20$, the values of $-\overline{\langle f_1 \rangle_{inc}}/\left\{u_\tau^2/h\right\}$ in the staggered arrays are larger than those in the square arrays. In addition, from Fig. 6, it is confirmed that, at all λ_p and heights, the values of $\langle \overline{u} \rangle_{inc}/u_\tau$ in the staggered arrays are smaller than those in the square arrays. Moreover, the values of $\langle \overline{u} \rangle_{inc}/u_\tau$ in the staggered arrays are more sensitive to λ_p than those in the square arrays, and they become very small in the square arrays with $\lambda_p \geq 0.25$. In other words, both the numerator and denominator in the right-hand side of Eq. 31 contribute to the increase in the sensitivity of $C_D(z)$ to λ_p in the staggered arrays.

Figure 12 shows the time-mean two-dimensional wind vectors $(\overline{u}, \overline{w})$ in the vertical $x-z$ planes at $y/h = 0.5$ and 0.75 (indicated in Fig. 7) for SQ25, SQ11, ST25a, and ST11. From

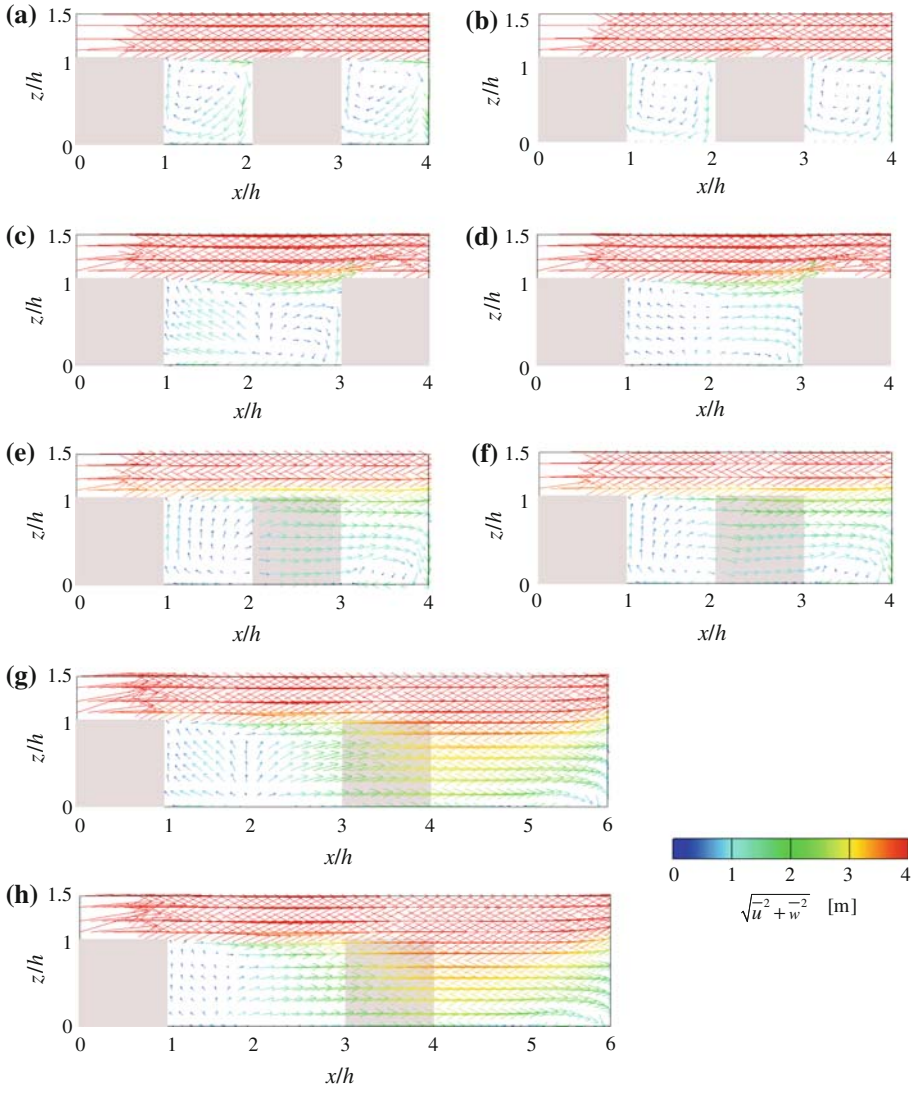

Fig. 12 Time-mean two-dimensional wind vectors $(\overline{u}, \overline{w})$ in vertical x–z plane: **a** SQ25 at $y/h = 0.5$ in Fig. 7c, **b** SQ25 at $y/h = 0.75$ in Fig. 7c, **c** SQ11 at $y/h = 0.5$ in Fig. 7f, **d** SQ11 at $y/h = 0.0.75$ in Fig. 7f, **e** ST25 at $y/h = 0.5$ in Fig. 7a, **f** ST25 at $y/h = 0.75$ in Fig. 7a, **g** ST11 at $y/h = 0.5$ in Fig. 7e, and **h** ST11 at $y/h = 0.75$ in Fig. 7e. The prevailing flow is to the right. The wind vectors are plotted at quarter resolution for greater clarity

Figs. 7 and 12, it is confirmed that the three-dimensional flow structure differs significantly in staggered arrays and in square arrays. With regard to the difference in the flow structures and pressure drag between staggered arrays and square arrays, Coceal et al. (2006) provided the following explanation for cube arrays with $\lambda_p = 0.25$ on the basis of their DNS results: "The cubes in the staggered configuration are further apart streamwise, hence there is less filtering. Moreover, the flow is diverted laterally because of staggered cubes in adjacent rows and speeds up in the gap, leading to greater pressure on the front face of the cubes. This

happens over most of the depth of the staggered array. In contrast, the close vicinity of cubes in the square arrays and the absence of lateral flow diversion mean that most of the momentum flux arises from the top. This has the consequence that the pressure drag profile for the staggered array is fuller (as shown in Fig. 11c, d)." With regard to the profile of $\langle\overline{u}\rangle_{inc}/u_\tau$, the discrepancy between that of the staggered array and square array is large at all heights, as shown in Fig. 6e; from Figs. 7a–d and 12a, b, e, f, it is understood that the smaller values of $\langle\overline{u}\rangle_{inc}/u_\tau$ in the staggered array as compared to the square array are due to the lateral flow diversion above $z/h = 0.2$, and the formation of recirculation vortices before and behind the cubes below $z/h = 0.2$. With a decrease in λ_p, the discrepancies in the profiles between the staggered arrays and square arrays become smaller for both $-\overline{\langle f_1\rangle_{inc}}/\left\{u_\tau^2/h\right\}$ and $\langle\overline{u}\rangle_{inc}/u_\tau$. In the staggered array with $\lambda_p = 0.11$, due to the reduced area ratio of the blocks' top surfaces and separated shear layers from them, the streamwise wind velocity becomes greater in front of the blocks as shown in Figs. 7e and 12g, h; together with the effect of the weakened recirculation vortices in front of the blocks, the profile of $-\overline{\langle f_1\rangle_{inc}}/\left\{u_\tau^2/h\right\}$ becomes fuller as shown in Fig. 11d. In the square arrays with $\lambda_p = 0.11$, in addition to the reduced filtering effects by the blocks' top surfaces, the contribution of the momentum flux from the lateral direction increases and the streamwise wind velocity becomes strong in front of the blocks as shown in Figs. 7f and 12d, resulting in the fuller profile of $-\overline{\langle f_1\rangle_{inc}}/\left\{u_\tau^2/h\right\}$ as shown in Fig. 11c.

5 Conclusions

In this study, we systematically investigated the properties of the spatially-averaged mean quantities used to make Macdonald's assumptions I–III by performing large-eddy simulations (LES) of the airflow around square and staggered arrays of cubical blocks with $\lambda_p =$ 0.05, 0.11, 0.16, 0.20, 0.25, and 0.33. The results are summarized as follows.

(i) Except for staggered arrays with $\lambda_p = 0.25$ and 0.33, the discrepancies between Macdonald's five-point average of wind velocity and the solid-inclusive average of wind velocity are smaller than those between Macdonald's five-point average of wind velocity and the solid-exclusive average of wind velocity. The values of the five-point average are significantly affected by the reverse flow region formed around blocks. In particular, in the lower part of square and staggered arrays with $\lambda_p \geq 0.25$, the values become extremely small as compared to those of the solid-inclusive or solid-exclusive averages. The attenuation coefficient obtained by fitting Macdonald's model equation to the wind profile of the five-point average and those of the solid-inclusive average can be approximated as a linear function of λ_p with similar slopes.

(ii) In all arrays, the values of l_m increase from the ground to around half the canopy height and then decrease to the canopy height. Subsequently, the values of l_m increase with height. As compared to the magnitude of l_m at twice the canopy height, the degrees of change in the values of l_m within the canopies are significantly large. The values of l_m become very small at around the height of the canopy because the values of $d\overline{\langle u\rangle}_{inc}/dz$ are significantly large at this height, although those of $\sqrt{-\overline{\langle uw\rangle}_{inc}}$ are maximum at around this height and turbulent transport is significant. With a decrease in λ_p, l_m decreases monotonically at around the height of the canopies. Within the canopies, the maximum and height-averaged values of l_m exhibit a peak at $\lambda_p = 0.11$ for square arrays and at $\lambda_p = 0.20$ for staggered arrays; between this and a lower value of λ_p, the maximum and height-averaged values of l_m decrease monotonically in both arrays.

(iii) The values of $C_D(z)$ are almost constant with height above $z/h \approx 0.1$ in square arrays with $\lambda_p \leq 0.25$ and above $z/h \approx 0.2$ in staggered arrays with $\lambda_p \leq 0.20$. While the values of $C_D(z)$ in the square arrays are insensitive to λ_p, those in the staggered arrays are sensitive to λ_p and become significantly large in staggered arrays with $\lambda_p \geq 0.25$. In staggered arrays, the values of $-\overline{\langle f_1 \rangle_{inc}}$ are generally larger as compared to those in square arrays, and the values of $\langle \overline{u} \rangle_{inc}$ are lower and more sensitive to λ_p; these tendencies lead to the higher sensitivity of $C_D(z)$ to λ_p in the staggered arrays than those in square arrays.

To develop a practical urban canopy model, it is necessary to understand the properties of spatially-averaged flow quantities within and above various types of urban canopies. In urban canopies with random building layouts and variable building heights, the five-point average would not be applicable. When a limited number of sampling points are available, it is important to evaluate the averaged value taking into account the volume of space occupied by buildings and the effects of reverse flow. With regard to l_m, the degrees of change in its values with height within the canopies would be smaller than those within the regular arrays of cubes, since the values of $d\overline{\langle u \rangle}_{inc}/dz$ at the canopy height (the height of the tallest building or the average building height) would be smaller due to the shear layers over buildings having various heights. With regard to $C_D(z)$, it is difficult to predict whether or not its values would be constant with height, since it depends on the balance between $-\overline{\langle f_1 \rangle_{inc}}$ and $\langle \overline{u} \rangle_{inc}^2$. For instance, in addition to the lateral flow diversion, which would be increased by a random arrangement of buildings, the reverse flow of the recirculation vortices around buildings can make the values of $\langle \overline{u} \rangle_{inc}^2$ very small; however, the relation between the formation of recirculation vortices and the urban canopies with random building layouts and variable building heights are not well known. Further investigations on the properties of spatially-averaged flow quantities within and above various types of urban canopies are required.

Acknowledgements We are grateful to Dr. Keiko Takahashi (The Earth Simulator Center, Japan) for providing us with the opportunity to use the Earth Simulator. We also would like to thank the anonymous three reviewers for their comments, which contributed to improving the presentation of the paper substantially. This research was supported by Core Research for Evaluation Science and Technology (CREST) of Japan Science and Technology Cooperation.

References

Amsden AA, Harlow FH (1970) A simplified MAC technique for incompressible fluid flow calculations. J Comput Phys 6:322–325

Castro IP, Cheng H, Reynolds R (2006) Turbulence over urban-type roughness: deduction from wind tunnel measurements. Boundary-Layer Meteorol 118:109–131

Cheng H, Castro IP (2002) Near wall flow over urban-like roughness. Boundary-Layer Meteorol 104:229–259

Cionco RM (1965) Mathematical model for air flow in a vegetative canopy. J Appl Meteorol 4:517–522

Coceal O, Belcher SE (2004) A canopy model of mean winds through urban areas. Q J Roy Meteorol Soc 130:1349–1372

Coceal O, Thomas TG, Castro IP, Belcher SE (2006) Mean flow and turbulence statistics over groups of urban-like cubical obstacles. Boundary-Layer Meteorol 121:491–519

Coceal O, Dobre A, Thomas TG, Belcher SE (2007) Structure of turbulent flow over regular arrays of cubical roughness. J Fluid Mech 589:375–409

ESDU (1986) Mean fluid forces and moments on rectangular prisms: surface-mounted structures in turbulent shear flow. Engineering Sciences Data Item Number 80003

Fadlun EA, Verzicco R, Orlandi P, Mohd-Yusof J (2000) Combined immersed-boundary finite-difference methods for three-dimensional complex flow simulations. J Comput Phys 161:35–60

Finnigan J (2000) Turbulence in plant canopies. Annu Rev Fluid Mech 32:519–571

Germano M, Piomelli U, Moin P, Cabot WH (1991) A dynamic subgrid-scale eddy viscosity in model. Phys Fluids A 3:1760–1765

Hamlyn D, Britter R (2005) A numerical study of the flow field and exchange processes within a canopy of urban-type roughness. Atmos Environ 39:3243–3254

Hanna SR, Tehranian S, Carissimo B, Macdonald RW, Lohner R (2002) Comparisons of model simulations with observations of mean flow and turbulence within simple obstacle arrays. Atmos Environ 36:5067–5079

Kanda M (2006) Large-eddy simulation on the effects of surface geometry of building arrays on turbulent organized structures. Boundary-Layer Meteorol 118:151–168

Kanda M, Moriwaki R, Kasamatsu F (2004) Large-eddy simulation of turbulent organized structures within and above explicitly resolved cube arrays. Boundary-Layer Meteorol 112:343–368

Kono T, Ashie Y, Tamura T (2007) Large eddy simulation of airflow around regular arrays of cubical buildings. In: APCOM'07 in conjunction with EPMESC XI, 3–6 December, Kyoto, Japan (MS4-2-3 in CD-ROM)

Kono T, Ashie Y, Tamura T (2009a) Derivation of spatially averaged momentum equations of multilayer urban canopy model using spatial-averaging operation corresponding to filtering operation of LES. Summaries of Technical Papers of Annual Meeting, Architectural Institute of Japan, 2009 D-1:949–950 (in Japanese)

Kono T, Ashie Y, Tamura T (2009b) Derivation of spatially averaged momentum equations of urban canopy model using the concept of the immersed boundary method. In: 7th international conference on urban climate, 29 June–3 July 2009, Yokohama, Japan (P3-21 in CD-ROM)

Leonard A (1974) Energy cascade in large-eddy simulations of turbulent fluid flows. Adv Geophys 18A:237–248

Lien F-S, Yee E, Wilson JD (2005) Numerical modelling of the turbulent flow developing within and over a 3-D building array, part II: a mathematical foundation for a distributed drag force approach. Boundary-Layer Meteorol 114:245–285

Lilly DK (1992) A proposed modification of the Germano subgrid-scale model. Phys Fluids A 4:633–635

Macdonald RW (2000) Modelling the mean velocity profile in the urban canopy layer. Boundary-Layer Meteorol 97:25–45

Miguel AF, van de Braak NJ, Silva AM, Bot GP (2001) Wind-induced airflow through permeable materials. Part 1: the motion equation. J Wind Eng Ind Aerodyn 89:45–57

Raupach MR, Shaw RH (1982) Averaging procedures for flow within vegetation canopies. Boundary-Layer Meteorol 22:79–90

Sabatino SD, Solazzo E, Paradisi P, Britter R (2008) A simple model for spatially-averaged wind profiles within and above an urban canopy. Boundary-Layer Meteorol 127:131–151

Sagaut P (2005) Large eddy simulation for incompressible flows, an introduction, 3rd edn. Springer, New York 15–31

Van der Vorst HA (1992) Bi-CGSTAB: a fast and smoothly converging variant of Bi-CG for the solution of nonsymmetric linear systems. SIAM J Sci Stat Comput 13(2):631–644